HHS Public Access

Author manuscript

Neurobiol Aging. Author manuscript; available in PMC 2016 June 01.

Published in final edited form as:

Neurobiol Aging. 2015 June ; 36(6): 2201–2212. doi:10.1016/j.neurobiolaging.2015.02.012.

Visual impairment in an optineurin mouse model of primary open angle glaucoma

Henry C. Tseng[1,*], **Thorfinn T. Riday**[2], **Celia McKee**[1], **Catherine E Braine**[3], **Howard Bomze**[1], **Ian Barak**[1], **Carrie Marean-Reardon**[1], **Simon W.M. John**[3,4,5], **Benjamin D. Philpot**[2], and **Michael D. Ehlers**[6,7]

[1]Duke Eye Center, Department of Ophthalmology, Duke University Medical Center, Durham, North Carolina 27710

[2]Department of Cell Biology and Physiology, Neuroscience Center, Carolina Institute for Developmental Disabilities, University of North Carolina School of Medicine, Chapel Hill, North Carolina 27599

[3]The Jackson Laboratory, 600 Main Street, Bar Harbor, ME 04609

[4]The Howard Hughes Medical Institute, The Jackson laboratory, 600 Main Street, Bar Harbor, ME 04609

[5]Department of Ophthalmology, Tufts University School of Medicine, Boston, MA 02111

[6]Department of Neurobiology and Howard Hughes Medical Institute, Duke University Medical Center, Durham, North Carolina 27710

Abstract

Primary open angle glaucoma (POAG) is characterized by progressive neurodegeneration of retinal ganglion cells (RGCs). Why RGCs degenerate in low pressure POAG remains poorly understood. To gain mechanistic insights, we developed a novel mouse model based on a mutation in human optineurin associated with hereditary, low-pressure POAG. This mouse improves the design and phenotype of currently available optineurin mice, which showed high global overexpression. While both 18-month old optineurin and nontransgenic control mice showed an age-related decrease in healthy axons and RGCs, the expression of mutant optineurin enhanced axonal degeneration and decreased RGC survival. Mouse visual function was determined using visual evoked potentials, which revealed specific visual impairment in contrast sensitivity. The E50K optineurin transgenic mouse described here exhibited clinical features of POAG, and may be useful for mechanistic dissection of POAG and therapeutic development.

[*]Address correspondence to: Henry C. Tseng Duke Eye Center 2351 Erwin Road, DUMC Box 3802 Durham, NC 27710 Phone: 919-684-8656 FAX: 919-681-8267 Henry.Tseng@duke.edu.

[7]Current address is: Pfizer Worldwide Research and Development, Neuroscience Research Unit, Cambridge, Massachusetts 02139

Keywords

POAG; neurodegeneration; optineurin; retinal ganglion cells; mouse model; vision

1. INTRODUCTION

Glaucoma is a leading cause of irreversible visual impairment and blindness (Quigley and Broman, 2006) resulting from progressive degeneration of retinal ganglion cells (RGCs) and optic neuropathy. Primary open angle glaucoma (POAG) is the predominant form in which no obvious clinical etiology is observed, and at least 50% of POAG patients worldwide exhibit low intraocular pressure (IOP) (Shields, 2008, Sommer, 2011). This presents a therapeutic challenge because all current glaucoma treatments function by lowering IOP. The precise pathophysiological mechanism of POAG remains unknown, but recent data suggest that RGC loss may occur through a neurodegenerative process similar to Alzheimer's disease, Huntington's disease, and amyotrophic lateral sclerosis (Bautista, 1999, Gupta and Yucel, 2007, Quigley, 2005).

Many existing animal models of glaucoma depend on inducing high IOP or trauma. For example, some models require laser injury or intraocular injection of saline or beads (Aihara, et al., 2003, Morrison, et al., 1997, Sappington, et al., 2010, WoldeMussie, et al., 2001). Other models require optic nerve crush or transection to injure RGC axons (Goldblum and Mittag, 2002, Tang, et al., 2011). A common genetic model (DBA/2J mouse) demonstrates abnormal pigment dispersion and iris atrophy that lead to an IOP elevation (Anderson, et al., 2005, Jakobs, et al., 2005). To study non-IOP risk factors and mechanisms that may contribute to RGC degeneration, a low-pressure POAG model is clearly needed.

Optineurin (OPTN) mutations have been associated with a loss of RGCs and motorneurons in familial low-pressure POAG and amyotrophic lateral sclerosis, respectively (Aung, et al., 2005, Maruyama, et al., 2010, Rezaie, et al., 2002). The E50K missense mutation in optineurin results in visual impairment in an autosomal dominant fashion, presumably due to a toxic gain of function mechanism. Transgenic mice with global overexpression of high levels of E50K mutant optineurin led to diffuse loss of photoreceptors and non-RGC cells, features not observed in POAG (Chi, et al., 2010, Meng, et al., 2011). We hypothesized that mice with low overexpression of E50K optineurin will more accurately reflect the phenotype observed in POAG patients (Rezaie, et al., 2002). Thus, we generated a different transgenic mouse using the genomic optineurin locus and promoter in a bacterial artificial chromosome (BAC). Near-physiological expression levels and subcellular localization have been reported with BACs (Heintz, 2000). The BAC E50K optineurin mouse model overcomes limitations of current optineurin and high-IOP glaucoma mouse models, and may be useful for studying early POAG pathophysiology.

2. MATERIALS AND METHODS

2.1 Mouse husbandry

All mouse experiments received approval from the Institutional Animal Care & Use Committee (IACUC) at both Duke University and the University of North Carolina (UNC), and were conducted according to Association for Research in Vision and Ophthalmology guidelines.

2.2 Generation of E50k human optineurin bacterial artificial chromosome transgenic mice

BAC transgenic constructs were generated by recombineering in *E. coli* (Yu, et al., 2000). The BAC clone RP11-1107F3 (Children's Hospital Oakland Research Institute) containing the 38 kb human optineurin locus with about 160 kb of 5' sequence was introduced into the bacterial strain EL250. Bacteria containing the BAC were transformed with two linear fragments: a 32-bp oligonucleotide (5-GAGCTCCTGACCAAGAACCACCAGCTGAAAGG-3) homologous to the 3' end of exon 4 and containing the E50K mutation in the middle (**G**AG → **A**AG), and a fragment containing IRES-EGFP followed by a Neomycin selection cassette and flanked by 50 bp homology arms for recombination immediately after the optineurin gene's translational stop sequence. The 5' homology sequence was 5-GCCTGACATAGACACGTTACAGATTC ACGTGATGGATTGCATCATTTAAGTG-3 while the 3' sequence was 5-GTATCACCTCCCCAAAACTGTTGGTAAATGTCAGATTTTTTCCTCCAAGAG-3.

Kanamycin-resistant BAC colonies were analyzed for homologous integration of the IRES-EGFP-neo cassette by PCR across the respective 5' and 3' homology arms. Incorporation of the mutant exon 4 sequence was verified by DNA dot blot hybridization of PCR fragments amplified with primers located 5' and 3' of the point mutation and probing with an oligonucleotide matching the wildtype and mutant sequence, respectively (wildtype: 5-CTCCTGACC**G**AGAACCACC-3; mutant: 5-CTCCTGACC**A**AGAACCACC-3) (Costa, et al., 2011). The frt-site flanked neo cassette was removed by arabinose induction of Flp recombinase in EL250. Field inversion gel electrophoresis (E) and DNA sequencing confirmed correct transgene construction and integrity of the BAC sequence. BAC DNA was linearized with NotI and purified by isotachophoresis (Ofverstedt, et al., 1984).

BAC DNA was injected into pronuclei of B6/SJL F1 zygotes at a concentration of 1 ng/μl. Potential founder mice were genotyped by tail DNA amplification using primers specific for the EGFP coding sequence. The following PCR primers were used for genotyping followed by DNA sequencing to confirm the E50K mutation: 5'-CATTCCTGCCCCAAGTGTGG-3' and 5'-GAATGCTCGTCAAGAAGACAGG-3'. Out of ~20 oocytes with the incorporated BAC transgene for E50K mutant human optineurin, two lines were successfully bred and backcrossed into the C57BL/6N background for 2-3 generations. BAC transgenic mice were aged along with wildtype nontransgenic littermates for 18 months.

2.3 qRT-PCR

Dissected retinas were snap-frozen with cold isopentane on dry ice before mRNA was isolated using RNeasy kits (Qiagen) and reverse-transcribed with the ProtoScript kit (New

England Biolabs) as per the manufacturers' directions. Results were normalized to housekeeping genes such as cyclophilin and GAPDH. Forward (F) and reverse (R) PCR primers are listed below: hOPTN-1 F: CACTGGCACGGCATTGTCTAA, R: CTGGGTTTCAATCTCAGAACGAT, hOPTN-2 F: AAAGAGCGTCTAATGGCCTTG, R: GTTCAGACACGATGCCCAACA, hOPTN-3 F: CCAAACCTGGACACGTTTACC, R: CCTCAAATCTCCCTTTCATGGC, mOPTN-1 F: TCAGGATGACCGAAGGAGAGA, R: TGGCTCACAGTCAGTTCTTCA, mOPTN-2 F: AGCAAAGAGGTTAAGGAGCGCCTTAAG, R: CAGCTTCTCCACTTCCTCCTCCAA, total OPTN-1: F: GGGAATCAGAAGGTGGAGAGACTTGAAGT, R: TGAGCCTCTTGAAGCTCCTTAAACAGAGA, Total OPTN-2 F: CCATCAGAGCTGAATGAAAAGCAAGAGCT, R: TGCCTTATTATGTTCTTGAAGGAGCTTGTTGTG, Cyclophin F: GAGCTGTTTGCAGACAAAGTTC, R: CCCTGGCACATGAATCCTGG, GAPDH: F: TGGCCTTCCGTGTTCCTAC, R: GAGTTGCTGTTGAAGTCGCA.

2.4 Immunoblot Analysis

Dissected retinas and brains were flash-frozen with chilled isopentane and stored at −80°C. Cell lysates were prepared in RIPA buffer containing protease inhibitors (Roche), and debris was cleared with ultracentrifugation. Standard SDS-polyacrylamide gel electrophoresis (SDS-PAGE) was performed before immunoblot detection with the Odyssey gel imaging system (Li-Cor Biosciences) with infrared detection. The following primary antibodies were used at 1:1000 dilution: rabbit OPTN-INT (Abcam), goat anti-OPTN-N (Santa Cruz Biotechnology), rabbit OPTN-C (Cayman Chemical), mouse FIP2 for optineurin (Transduction Laboratory), and rabbit beta-actin (Sigma).

2.5 Intraocular Pressure Measurement

IOP was measured with a rebound tonometer (iCare Technologies) per manufacturer's directions. Since anesthesia is known to alter IOP in both patients and mice (Cone, et al., 2012), IOP measurements were taken as soon as the mice were sedated sufficiently to remain still. At least three measurements were taken per eye per animal. Average values were analyzed for statistical significance using Student's t-test.

2.6 Immunohistochemistry of retina cryosections

14 micron sections of retinas were stained using standard immunostaining approach. Briefly, the sections were blocked with 4% donkey serum before being incubated in primary antibody overnight at 4°C and secondary antibody the next day. The retina sections were imaged using a confocal fluorescence microscope. The following antibodies and dilutions were utilized: mouse SMI-32 antibody for neurofilament (Covance) 1:2000, rabbit anti-protein kinase C alpha (Sigma) 1:1000, mouse anti-calretinin (Millipore) 1:1000, rabbit anti-OPTN-INT (Cayman Chemical) 1:200, and rabbit anti-OPTN-C (Cayman Chemical) 1:200.

2.7 Quantitation of retinal layer thickness

Measurements of each retinal layer and total retinal thickness were performed using confocal microscope images of retina sections. Central retina measurements were made 200

m from the optic nerve. Peripheral retina measurements were taken 200 μm away from the edge of the peripheral retina within the same section. The photoreceptor outer segment layer was not quantified due to occasional artifactual retinal detachment resulting from histological preparation. Nuclear layers were defined by DAPI staining while the plexiform layers were defined as the region in between the DAPI staining.

2.8 Immunohistochemistry of retina flatmount and RGC count

After transcardial perfusion with cold 4% paraformaldehyde, the retina was carefully dissected, blocked in 4% donkey serum in 0.1% triton/PBS, incubated in primary antibody at 4°C for 3-5 days, and stained with secondary antibody at 4°C. Mouse SMI-32 antibody for neurofilament (Covance) was used at a 1:2000 dilution. Multiple tiled images taken with a confocal fluorescence microscope were assembled into a mosaic image that covered the entire retina flatmount (See brain imaging section below). Counts were performed in a blinded fashion within a rectangular region that was 0.25 mm^2 in area (500 m × 500 m grid) at 1.5 mm from the optic nerve. Counts were made from all four quadrants of each retina flatmount in a blinded fashion. RGC densities were calculated and compared for statistical significance using the Student's t-test.

2.9 Quantification of Axons in Optic Nerves

Staining for damaged/dead axons in optic nerve cross sections was performed using a modified paraphenylenediamine (PPD) protocol as previously described (Anderson, et al., 2005). Axon counting was performed in 20 non-overlapping representative areas of each nerve cross section at x100 magnification. PPD stains all axonal myelin sheath, but darkly stains the axoplasm of damaged or dead axons. Axons with and without PPD staining in axoplasm were counted to evaluate “damaged/dead” and “healthy” axons, respectively, in a blinded fashion. The Student's t-test was utilized to assess statistical significance.

2.10 Cholera-toxin labeling of retinal ganglion cells

Retinal ganglion cell axonal terminals in the brain were labeled in an anterograde fashion by injecting fluorescently-labeled recombinant cholera toxin into the eye. Cholera toxin conjugated to Alexa Fluor 555 or Alexa Fluor 647 (Life Technologies, formerly Invitrogen) at a concentration of 1.0 mg/mL in PBS were injected intraocularly through a 33-gauge canula. 1μl of the cholera toxin solution was delivered slowly and in a controlled fashion into the eye over 60 seconds using a QSI microprocessor-controlled injector (Stoelting Company) to avoid IOP spikes. Mice were killed 2-3 days later to harvest eye and brain tissue for histological evaluation.

2.11 Imaging of brain sections

Serial 30 μm brain sections were cut using a cryostat in either a coronal or sagittal orientation. Fluorescently-labeled cholera toxin in brain sections were imaged utilizing either a Zeiss LSM 510 Inverted Confocal Fluorescence Microscope equipped with a motorized stage (Marzhauser scan stage) or a Zeiss Axio Imager with a motorized stage. Entire brain sections were imaged with a 5x objective, and multiple tiled images were assembled into a mosaic.

2.12 Visual Evoked Potential (VEP) recording

Mice were implanted with four intracranial electrodes. After craniotomies were drilled with a 0.5 mm diameter burr while suspended in a stereotaxic frame, tungsten microelectrodes (0.3-0.5 MΩ; FHC) were bilaterally implanted in V1 visual cortex, ±3.00 mm lateral to lambda and 0.45 mm below the brain surface. Silver reference electrodes were implanted at the brain surface, ±2.00 mm lateral and 1.0 mm posterior to bregma. Electrodes and holding post (resting on the skull surface anterior to bregma) were secured to the skull with cyanoacrylate (Henkel).

After electrode implantation, mice were given at least 48 hours for recovery. All mice were first habituated to the head restraint apparatus 24 hours before VEP recording sessions. Awake, non-anesthetized mice were positioned 20 cm from a 21 inch CRT monitor (80 cd/m^2) that displayed computer-generated visual stimuli. Their heads were fixed toward the computer monitor by the holding post that was attached to the skull as described above.

Mice were presented with 100% contrast gratings at different spatial frequencies. Visual acuity is expressed as spatial frequency of cycles per degree (cpd), where one cycle is defined to include a black and white grating. These gratings were rotated 90 degrees on each repeated trial to minimize stimulus-selective response potentiation, a phenomenon whereby the repeated presentation of the same stimulus can potentiate responses to that selective stimulus (Frenkel, et al., 2006). Visual stimuli consisted of full-field square counterphase sine gratings (45° or 135°) with a 1 Hz reversal frequency (Vision Research Graphics). Data from every implanted mouse were included in the results, using the electrode (1 of 2) that generated the larger VEP for 0.05 cpd at 100 % contrast. Visual acuity (0.0, 0.05, 0.15, 0.25, 0.35, 0.45. 0.55, 0.65, 0.75, 0.85, 0.95, 2.84 cpd at 100% contrast) and contrast sensitivity (100, 50, 25, 12, 6, 3, 1.5, 0.8, 0.4, 0.2, 0.1, 0.0 % at 0.05 cpd) were determined by the trough to peak VEP amplitude of 102 averaged responses per condition (3 blocks of 34 stimuli presented in random order with 10 sec breaks). Visual thresholds were determined for individual mice using logarithmic (contrast sensitivity) and linear (visual acuity) regression analysis interpolated into the noise level (gray screen response). All recordings were amplified 1000x, and high and low band filtered at 0.1 Hz and 100 Hz (Grass Instruments). Recordings were acquired in with a Micro 1401-3 digitizer in combination with Spike2 (Cambridge Electronic Design). The data were analyzed by two-way repeated measures ANOVA for statistical significance.

3. RESULTS

3.1 Generation of transgenic mice with low overexpression of E50K human optineurin

A BAC that contained the optineurin promoter region and genomic human *OPTN* gene was used (Figure 1A). Resultant transgenic lines (BAC-hOPTN$^{E50K)}$ were maintained as heterozygotes, similar to genotypes of reported POAG patients with the E50K mutation (Aung, et al., 2005, Rezaie, et al., 2002).

qRT-PCR was used to assess optineurin mRNA expression levels in isolated retinas from 18 month-old BAC-hOPTN^{E50K} mice (Figure 1B). E50K hOPTN mRNAs were expressed in BAC-hOPTN^{E50K} mice, but not retinas from wildtype littermates, and was 3-fold higher in

the first BAC transgenic line compared to the second line. Using mouse-specific PCR primers, we found that endogenous mouse optineurin expression levels were similar among all genotypes, indicating that the mutant E50K human optineurin transgene does not affect endogenous mouse optineurin expression. Primers that recognize both human and mouse optineurin showed that total optineurin expression was 1.3-fold higher in line 1 of BAC-hOPTN^{E50K} mice than wildtype nontransgenic mice.

Protein levels for E50K hOPTN were assessed using dissected retinas in immunoblot analysis (Figure 1C). Using an antibody that recognizes only human optineurin, E50K hOPTN was found in both young (2-3 month old, data not shown) and old (18 month old, Figure 1C) BAC-hOPTN^{E50K} mice. As expected, no expression of human optineurin was observed in retinas from wildtype control littermates. Both mRNA and protein expression data show that line 1 of BAC-hOPTN^{E50K} mice is best suitable for characterization experiments; subsequent references of BAC-hOPTN^{E50K} below refer to this line.

3.2 E50K optineurin mice exhibit normal eye anatomy and intraocular pressure

We performed slit-lamp biomicroscopy and found no gross clinical abnormalities in BAC-hOPTN^{E50K} eyes (data not shown). Features found in the DBA/2J glaucoma mouse model, such as prominent pigment dispersion and iris atrophy, were not observed in BAC-hOPTN^{E50K} mice even after 18 months of age.

IOP > 21-22 is often clinially regarded as a glaucoma risk factor clinically and in glaucoma mouse animal models (Anderson, et al., 2006, Savinova, et al., 2001). IOP for young (2-3 months, n = 5 per genotype) and aged (18 months, n = 10 per genotype) BAC-hOPTN^{E50K} mice were compared to wildtype littermate controls (Figure 1D). In young BAC-hOPTN^{E50K} mice, the IOP was 10.6 ± 0.7 mmHg (mean ± S.E.M.) in the right eye (OD) and 10.5 ± 0.5 mmHg in the left eye (OS). This is similar to 10.5 ± 0.4 OD and 10.5 ± 0.8 OS for wildtype control mice ($p = 0.77$). In 18-month old mice, IOP was 8.4 ± 0.4 mmHg OD and 8.0 ± 0.7 mmHg OS for BAC-hOPTN^{E50K} mice and 8.6 ± 0.4 mmHg OD and 9.0 ± 0.5 mmHg OS for wildtype littermates (Figure 1D). No asymmetries were observed in IOP between the right and left eyes for any of the genotypes (p values ranged from 0.2 to 0.7), another clinical risk factor for glaucoma. The age-related decrease in IOP are consistent with literature reports (Savinova, et al., 2001).

3.3 Localization of E50K hOPTN expression in the retina

Because the expression of E50K human optineurin is driven by a genomic optineurin promoter, its expression pattern in the retina should resemble that of endogenous optineurin. To assess this, we performed immunolabeling of retina sections from 18-month-old BAC-hOPTN^{E50K} mice. Brn3a was used to identify RGC nuclei, while DAPI nuclear stain was used to identify the ganglion cell layer (GCL), inner nuclear layer (INL), and outer nuclear layer (ONL). Using an antibody specific for human optineurin, we did not detect labeling in wildtype retinas (Figure 1E, top panels). In contrast, in BAC-hOPTN^{E50K} retinas, expression of human E50K optineurin was observed in the ganglion cell layer and the outer plexiform layer (OPL). The same immunostaining pattern was observed using an antibody

that recognizes both mouse and human optineurin. The staining pattern with this antibody is identical in both BAC-hOPTN^{E50K} and wildtype retinas (Figure 1E, bottom panels).

3.4 Low E50K human optineurin expression does not lead to diffuse loss of retinal layers

In optineurin mice with high, ubiquitous overexpression of E50K hOPTN, diffuse loss of non-GFL layers resulted in ~ 50% thinner retinas (Chi, et al., 2010). These features are not observed in POAG patients (Wax, et al., 1998). Qualitative and quantitative evaluation for retinal thickness was performed in BAC-hOPTN^{E50K} (n = 3 animals) and wildtype (n = 4 animals) retina sections (Figure 2A, 2B). Total retinal thickness was 177 ± 8 m centrally (mean ± S.E.M.) and 132 ± 1 m peripherally for BAC-hOPTN^{E50K} mice, which are similar to wildtype mice (184 ± 5 m centrally, 129 ± 20 m peripherally). Individual retinal layers revealed no significant thickness differences between BAC-hOPTN^{E50K} and wildtype littermate mice, with the exception of an increasing trend in the thickness of the RGL and ONL in the peripheral retina of BAC-hOPTN^{E50K} mice. Taken together, our data demonstrate minimal thinning in non-GCL layers in BAC-hOPTN^{E50K} mice.

3.5 Axonal targeting of retinal ganglion cells in the brain is unaffected by E50K human optineurin

RGC axons exit the eye as the optic nerve and terminate at the lateral genicual nucleus and the superior colliculus. To assess whether E50K human optineurin disrupts this RGC anatomy centrally, we examined the brain after intraocular injections of fluorescently-labeled cholera toxin as an anterograde tracer (Huberman, et al., 2009) in old BAC-hOPTN^{E50K} and wildtype mice (n = 3 animals per genotypes). In coronal brain sections from BAC-hOPTN^{E50K} mice, RGC axon terminals were detected in the superior colliculus and lateral geniculate nucleus, indistinguishable from wildtype mice. When each eye was injected with a different fluorescent tracer, distinct ipsilateral and contralateral RGC axonal projections were visualized at a small binocular zone in the lateral geniculate nucleus (Figure 2C). Sagittal brain sections also localized RGC axon terminals to the superior colliculus (Figure 2D). Therefore, E50K optineurin does not alter RGC axonal pathfinding in the brain.

3.6 Age-related loss of retinal ganglion cells in mice with E50K human optineurin

A key histological feature of POAG is age-related loss of RGCs; thus we next compared the number of RGCs in BAC-hOPTN^{E50K} mouse retinas to wildtype retinas. While many RGC markers have been reported, none are completely specific for RGCs (Coombs, et al., 2006, Diao, et al., 2004, Sun, et al., 2002). We used the well-established standard of SMI-32 antibody (Jakobs, et al., 2005, Lin, et al., 2004) to identify a subset of representative RGCs in retina flatmount for cell counting.

Representative retina flatmounts from young (2-3 months) and aged (>18 months) mice are shown for BAC-hOPTN^{E50K} mice and wildtype littermates in Figure 3A. In both young BAC-hOPTN^{E50K} and wildtype mice, retina flatmounts revealed that RGC soma and axons are robustly labeled by SMI-32 and appeared morphologically healthy. RGC axons were readily identified as they extend toward the optic nerve located at the center of the mouse retina. In contrast, retinas from older mice exhibited an overall reduction in SMI-32 labeled

RGCs in both BAC-hOPTN^{E50K} and wildtype mice. However, the reduction in aged BAC-hOPTN^{E50K} mice was more pronounced.

Quantitative analysis of RGC cell density revealed that BAC-hOPTN^{E50K} retinas showed RGC loss that was greater than expected for normal, age-related attrition (Figure 3B). A comparison between the two genotypes revealed no difference in RGCs between young BAC-hOPTN^{E50K} and wildtype controls (mean ± S.E.M.; wildtype 166 ± 18 RGCs per mm^2; BAC-hOPTN^{E50K} 190 ± 19 RGCs per mm^2; $p = 0.38$). In contrast, 18-month-old mice expressing E50K mutant optineurin had a significant decrease (~40%) in RGC density relative to wildtype littermates (wildtype 124 ± 9 RGCs per mm^2; BAC-hOPTN^{E50K} 76 ± 14 RGCs per mm^2; $p<0.02$). The age-related decreased in RGC survival was more pronounced in BAC-hOPTN^{E50K} mice ($p = 0.001$) than in wildtype mice ($p = 0.07$). Taken together, the expression of mutant E50K optineurin enhanced aged-dependent RGC loss.

3.7 Mutant optineurin induces more axonal damage

We next determined if differential loss of RGCs in 18-month old BAC-hOPTN^{E50K} mice is associated with axonal damage or loss. In aged BAC-hOPTN^{E50K} (n = 4 animals, 8 optic nerves) and nontransgenic wildtype littermate (n = 6 animals, 11 optic nerves) mice, paraphenylenediamine (PPD) staining was performed in optic nerve sections (Figure 4A). PPD stains axonal myelin sheath to facilitate visualization of axonal cross-sections for counting. Also, PPD darkly stains the axoplasm of stressed or degenerating axons (Anderson, et al., 2005).

By counting axons with a clear axoplasm, the number of “healthy” axons was assessed (Figure 4B). No statistically-significant difference was observed as optic nerves from both genotypes showed similar number of healthy axons (mean ± S.E.M.; 32,258 ± 2,338 for BAC-hOPTN^{E50K} and 28,445 ± 2,740 for wildtype mice; $p = 0.33$). Quantitation of PPD-stained axons (Figure 4C) showed that there are more stressed or degenerating axons in optic nerves from BAC-hOPTN^{E50K} than wildtype mice (mean ± SEM; 1235 ± 152 for BAC-hOPTN^{E50K} and 684 ±170 for wildtype; $p = 0.03$). Thus the data revealed that although age-dependent RGC loss occurred in both BAC-hOPTN^{E50K} and nontransgenic mice after 18 months, E50K hOPTN induced a larger number of stressed or degenerating axons.

3.8 Functional visual impairment in BAC E50K optineurin mice

We next assessed visual function by measuring visual-evoked potential (VEPs) directly from electrodes implanted in the visual cortex in non-anesthesized mice (Cho, et al., 2009, Frenkel and Bear, 2004). Aged 18-month BAC-hOPTN^{E50K} mice (n = 8 animals) exhibited a significant decrease in contrast sensitivity relative to wildtype littermates (n = 11 animals) across a range of contrasts ($p<0.05$ to 0.005; Figure 5A) although acuity thresholds were similar between the two genotypes. The visual acuity threshold (E50K, 0.56 cpd, n = 8; WT, 0.58 cpd, n = 11; Figure 5B) was comparable to the 0.6 cpd reported in the literature (Porciatti, et al., 2002, Prusky, et al., 2000). Despite normal acuity thresholds, aged BAC-hOPTN^{E50K} mice did exhibit an attenuated visual acuity response at 0.05 cpd as compared to wildtype littermates, but not other acuity levels (Figure 5B).

Because nerve conduction and axon potential propagation is impaired in many optic nerve diseases, we also measured the latency between the presentation of a visual stimulus and the detection of the initial electrophysiological response (Gow, et al., 1999, Strain and Tedford, 1993). The latency of visual responses is based on time to initiation of the VEP response ("Time to VEP"), latency to the first maximal response ("Time to N1"), and latency to the second maximal response ("Time to P1"). Both BAC-hOPTN^{E50K} (n = 8 animals) and wildtype littermate mice (n = 11 animals) exhibited similar latencies (Figure 5C). The "Time to VEP," "Time to N1," and "Time to P1" were 20.45 ms ± 0.36, 41.45 ms ± 2.32, and 116.99 ms ± 6.00 for BAC-hOPTN^{E50K} and 21.71 ms ± 0.47, 43.17 ms ± 0.84, and 113.28 ms ± 3.08 for wildtype littermates (mean ± S.E.M.). None of these measurements were significantly different between genotypes. Taken together, intracranial VEP responses show that low-overexpression of E50K mutant human optineurin results in selective visual impairment in contrast sensitivity, but does not have a quantifiable effect on nerve conduction velocity.

4. DISCUSSION

4.1 POAG phenotype with low overexpression of E50K optineurin

POAG disease findings include functional visual impairment, loss of RGCs, no loss of other retinal cell types such as photoreceptors, and a normal gross eye anatomy without pathological features such as angle closure, pigment dispersion, inflammation, or trauma (AAO, 2010, Kendell, et al., 1995, Kerrigan, et al., 1997, Quigley, 1999, Wax, et al., 1998). These clinical features and low IOP were observed in BAC-hOPTN^{E50K} mice. In contrast to optineurin mice in previous reports, no diffuse thinning of non-GCL layers was found (Chi, et al., 2010, Meng, et al., 2011).

While significant RGC and axonal loss (>80-90%) is typically reported in high-pressure glaucoma animal models, it is not surprising that BAC-hOPTN^{E50K} mice showed a mild glaucoma phenotype. First, without high IOP, progressive RGC neurodegeneration likely occurred at a slower rate and possibly through a different disease mechanism. Second, BAC-hOPTN^{E50K} mice also express normal mouse OPTN alleles, which may partially compensate for disrupted biochemical pathways resulting from E50K optineurin. Thus, we predict greater RGC loss in BAC-hOPTN^{E50K} mice with suppression of endogenous normal mouse OPTN as well as additional glaucoma stressors, such as increased IOP.

4.2 Assessing neurodegeneration in POAG

The lack of a reliable marker limits quantitative assessment of RGC loss in any glaucoma mouse model. Recent reports have identified >20 RGC subtypes that can be identified electrophysiologically or morphologically, but no specific biochemical markers have been identified for each RGC subtype or for all RGCs in general (Coombs, et al., 2006, Sun, et al., 2002). The use of the SMI-32 antibody to morphologically identify a subset of RGCs (Coombs, et al., 2006) to assess representative RGC loss in mice is well-established (Jakobs, et al., 2005, Lin and Peng, 2013). Using the SMI-32 antibody, our RGC density measurement in wildtype retinas are comparable to literature reports of 80-110 RGCs per

mm^2 (Lin and Peng, 2013, Lin, et al., 2004). With the four intracranial VEP electrode implants, retrograde labeling of RGCs was not possible in our experiments.

Another approach for estimating RGC loss in glaucoma is counting RGC axons in the optic nerve after PPD staining (Anderson, et al., 2005, Howell, et al., 2007). We found a higher number of PPD-stained axons in aged BAC-hOPTN^{E50K} mice than wildtype ones. Interestingly, both genotypes have fewer "healthy" axons than previous reports, which ranged from 4.06×10^4 (Inman, et al., 2006), 4.8×10^4 (Jeon, et al., 1998), 5.46×10^4 (Williams, et al., 1996), and 5.7×10^4 axons (Mabuchi, et al., 2004). Thus, our data showed an age-related loss of RGCs in both genotypes, which is enhanced by E50K hOPTN expression as evidenced by PPD staining and RGC counts. It is possible a subset of "healthy" axons in BAC-hOPTN^{E50K} mice might be dysfunctional, but not sufficiently enough to be stained by PPD.

We performed VEPs to assess visual function in BAC-hOPTN^{E50K} mice. It is notable that visual impairment in BAC-hOPTN^{E50K} mice was quite specific for one visual modality (contrast sensitivity) but less for another (visual acuity). This VEP finding is consistent with the clinical presentation of POAG (Abdullah, et al., 2014, Horn, et al., 2006, Quigley, 1999, Tyler, 1981). Additionally, BAC-hOPTN^{E50K} mice exhibited normal conduction velocity. While no demyelinating pathology is found in the optic nerve of POAG patients (Quigley and Green, 1979), it remains to be determined whether POAG patients exhibit delayed VEP latency. Depending on study methodology and patient population, both clinically significant and insignificant latencies have been reported (Grippo, et al., 2006, Horn, et al., 2006, Parisi, et al., 2006).

4.3 Possible neurodegenerative disease mechanisms in POAG

The pathophysiology for POAG remains remarkably elusive, but studying OPTN's *in vivo* role may lead to mechanistic clues. Disrupted protein trafficking has been proposed as a glaucoma disease mechanism (Quigley and Addicks, 1980), and optineurin itself functions as an adaptor protein for motor-based vesicular transport (Chibalina, et al., 2010, Chibalina, et al., 2008, Sahlender, et al., 2005). Loss of OPTN in zebrafish disrupts axonal trafficking in the spinal cord (Paulus and Link, 2014), and OPTN knockdown results in loss of cultured neurons (Akizuki, et al., 2013). Alternatively, optineurin might alter NFκB activity (Sudhakar, et al., 2009, Zhu, et al., 2007). Signaling components of the NFκB pathway, such as TNFα and TBK1, are also associated with glaucoma and interacts with optineurin (Klingseisen, et al., 2012, Morton, et al., 2008, Tezel, et al., 2001). Other functions for optineurin include: a K63-polyubiquitin-chain binding protein (Nagabhushana, et al., 2011, Zhu, et al., 2007), a negative checkpoint for cytokinesis (Kachaner, et al., 2012), and an autophagy/mitophagy receptor (Korac, et al., 2013, Wild, et al., 2011, Wong and Holzbaur, 2014). The BAC-hOPTN^{E50K} mouse can facilitate future investigations into these pathways.

In summary, we have generated and characterized an optineurin mouse that will help define the pathophysiology of RGC degeneration in low-pressure POAG. Future work may reveal novel molecules that can be exploited as disease biomarkers or therapeutic targets. More broadly, given optineurin's genetic association with familial amyotrophic lateral sclerosis and potential involvement in Huntington's and Alzheimer's diseases (Liu and Tian, 2011,

Mori, et al., 2012, Osawa, et al., 2011), elucidating *in vivo* mechanisms of optineurin-associated RGC loss in glaucoma may also reveal mechanistic insights and therapeutic strategies for other neurodegenerative diseases.

ACKNOWLEDGEMENTS

We thank Marc Caron and the Duke Neurotransgenic Laboratory for assistance. We acknowledge funding from: K12-EY016333 & K08-EY021520 (HCT), American Glaucoma Society (HCT), Butler Pioneer Award (HCT), the Howard Hughes Medical Institute (MDE & SWMJ), R01-EY11721 (SWMJ), R01-EY018323 (BDP), and an NEI core grant P30-EY005722 to the Duke Eye Center. Data were partially presented at the 2014 Association for Research in Vision and Ophthalmology (ARVO) meeting. Michael Ehlers is an employee and shareholder of Pfizer, Inc. All remaining authors declare no competing financial interests.

REFERENCES

AAO. Primary Open-Angle Glaucoma. American Academy of Ophthalmology Preferred Practice Pattern. 2010

Abdullah SN, Sanderson GF, James AC, Vaegan, Maddess T. Visual evoked potential and psychophysical contrast thresholds in glaucoma. Doc Ophthalmol. 2014; 128(2):111–20. [PubMed: 24615592]

Aihara M, Lindsey JD, Weinreb RN. Experimental mouse ocular hypertension: establishment of the model. Invest Ophthalmol Vis Sci. 2003; 44(10):4314–20. [PubMed: 14507875]

Akizuki M, Yamashita H, Uemura K, Maruyama H, Kawakami H, Ito H, Takahashi R. Optineurin suppression causes neuronal cell death via NF-kappaB pathway. J Neurochem. 2013

Anderson MG, Libby RT, Gould DB, Smith RS, John SW. High-dose radiation with bone marrow transfer prevents neurodegeneration in an inherited glaucoma. Proc Natl Acad Sci U S A. 2005; 102(12):4566–71. [PubMed: 15758074]

Anderson MG, Libby RT, Mao M, Cosma IM, Wilson LA, Smith RS, John SW. Genetic context determines susceptibility to intraocular pressure elevation in a mouse pigmentary glaucoma. BMC biology. 2006; 4:20. [PubMed: 16827931]

Aung T, Rezaie T, Okada K, Viswanathan AC, Child AH, Brice G, Bhattacharya SS, Lehmann OJ, Sarfarazi M, Hitchings RA. Clinical features and course of patients with glaucoma with the E50K mutation in the optineurin gene. Invest Ophthalmol Vis Sci. 2005; 46(8):2816–22. [PubMed: 16043855]

Bautista RD. Glaucomatous neurodegeneration and the concept of neuroprotection. International ophthalmology clinics. 1999; 39(3):57–70. [PubMed: 10709574]

Chi ZL, Akahori M, Obazawa M, Minami M, Noda T, Nakaya N, Tomarev S, Kawase K, Yamamoto T, Noda S, Sasaoka M, Shimazaki A, Takada Y, Iwata T. Overexpression of optineurin E50K disrupts Rab8 interaction and leads to a progressive retinal degeneration in mice. Hum Mol Genet. 2010

Chibalina MV, Poliakov A, Kendrick-Jones J, Buss F. Myosin VI and optineurin are required for polarized EGFR delivery and directed migration. Traffic. 2010; 11(10):1290–303. [PubMed: 20604900]

Chibalina MV, Roberts RC, Arden SD, Kendrick-Jones J, Buss F. Rab8-optineurin-myosin VI: analysis of interactions and functions in the secretory pathway. Methods Enzymol. 2008; 438:11–24. [PubMed: 18413238]

Cho KK, Khibnik L, Philpot BD, Bear MF. The ratio of NR2A/B NMDA receptor subunits determines the qualities of ocular dominance plasticity in visual cortex. Proc Natl Acad Sci U S A. 2009; 106(13):5377–82. [PubMed: 19276107]

Cone FE, Steinhart MR, Oglesby EN, Kalesnykas G, Pease ME, Quigley HA. The effects of anesthesia, mouse strain and age on intraocular pressure and an improved murine model of experimental glaucoma. Exp Eye Res. 2012; 99:27–35. [PubMed: 22554836]

Coombs J, van der List D, Wang GY, Chalupa LM. Morphological properties of mouse retinal ganglion cells. Neuroscience. 2006; 140(1):123–36. [PubMed: 16626866]

Costa JL, Forbes S, Brennan MB, Hochgeschwender U. Genetic modifications of mouse proopiomelanocortin peptide processing. Mol Cell Endocrinol. 2011; 336(1-2):14–22. [PubMed: 21195130]

Diao L, Sun W, Deng Q, He S. Development of the mouse retina: emerging morphological diversity of the ganglion cells. J Neurobiol. 2004; 61(2):236–49. [PubMed: 15389605]

Frenkel MY, Bear MF. How monocular deprivation shifts ocular dominance in visual cortex of young mice. Neuron. 2004; 44(6):917–23. [PubMed: 15603735]

Frenkel MY, Sawtell NB, Diogo AC, Yoon B, Neve RL, Bear MF. Instructive effect of visual experience in mouse visual cortex. Neuron. 2006; 51(3):339–49. [PubMed: 16880128]

Goldblum D, Mittag T. Prospects for relevant glaucoma models with retinal ganglion cell damage in the rodent eye. Vision Res. 2002; 42(4):471–8. [PubMed: 11853763]

Gow A, Southwood CM, Li JS, Pariali M, Riordan GP, Brodie SE, Danias J, Bronstein JM, Kachar B, Lazzarini RA. CNS myelin and sertoli cell tight junction strands are absent in Osp/claudin-11 null mice. Cell. 1999; 99(6):649–59. [PubMed: 10612400]

Grippo TM, Hood DC, Kanadani FN, Ezon I, Greenstein VC, Liebmann JM, Ritch R. A comparison between multifocal and conventional VEP latency changes secondary to glaucomatous damage. Invest Ophthalmol Vis Sci. 2006; 47(12):5331–6. [PubMed: 17122121]

Gupta N, Yucel YH. Glaucoma as a neurodegenerative disease. Current opinion in ophthalmology. 2007; 18(2):110–4. [PubMed: 17301611]

Heintz N. Analysis of mammalian central nervous system gene expression and function using bacterial artificial chromosome-mediated transgenesis. Hum Mol Genet. 2000; 9(6):937–43. [PubMed: 10767317]

Horn FK, Michelson G, Schnitzler E, Mardin CY, Korth M, Junemann AG. Visual evoked potentials of the blue-sensitive pathway under cold provocation in normals and glaucomas. J Glaucoma. 2006; 15(1):17–22. [PubMed: 16378012]

Howell GR, Libby RT, Jakobs TC, Smith RS, Phalan FC, Barter JW, Barbay JM, Marchant JK, Mahesh N, Porciatti V, Whitmore AV, Masland RH, John SW. Axons of retinal ganglion cells are insulted in the optic nerve early in DBA/2J glaucoma. J Cell Biol. 2007; 179(7):1523–37. [PubMed: 18158332]

Huberman AD, Wei W, Elstrott J, Stafford BK, Feller MB, Barres BA. Genetic identification of an On-Off direction-selective retinal ganglion cell subtype reveals a layer-specific subcortical map of posterior motion. Neuron. 2009; 62(3):327–34. [PubMed: 19447089]

Inman DM, Sappington RM, Horner PJ, Calkins DJ. Quantitative correlation of optic nerve pathology with ocular pressure and corneal thickness in the DBA/2 mouse model of glaucoma. Invest Ophthalmol Vis Sci. 2006; 47(3):986–96. [PubMed: 16505033]

Jakobs TC, Libby RT, Ben Y, John SW, Masland RH. Retinal ganglion cell degeneration is topological but not cell type specific in DBA/2J mice. J Cell Biol. 2005; 171(2):313–25. [PubMed: 16247030]

Jeon CJ, Strettoi E, Masland RH. The major cell populations of the mouse retina. J Neurosci. 1998; 18(21):8936–46. [PubMed: 9786999]

Kachaner D, Filipe J, Laplantine E, Bauch A, Bennett KL, Superti-Furga G, Israel A, Weil R. Plk1-dependent phosphorylation of optineurin provides a negative feedback mechanism for mitotic progression. Mol Cell. 2012; 45(4):553–66. [PubMed: 22365832]

Kendell KR, Quigley HA, Kerrigan LA, Pease ME, Quigley EN. Primary open-angle glaucoma is not associated with photoreceptor loss. Invest Ophthalmol Vis Sci. 1995; 36(1):200–5. [PubMed: 7822147]

Kerrigan LA, Zack DJ, Quigley HA, Smith SD, Pease ME. TUNEL-positive ganglion cells in human primary open-angle glaucoma. Arch Ophthalmol. 1997; 115(8):1031–5. [PubMed: 9258226]

Klingseisen L, Ehrenschwender M, Heigl U, Wajant H, Hehlgans T, Schutze S, Schneider-Brachert W. E3-14.7K is recruited to TNF-receptor 1 and blocks TNF cytolysis independent from interaction with optineurin. PLoS ONE. 2012; 7(6):e38348. [PubMed: 22675546]

Korac J, Schaeffer V, Kovacevic I, Clement AM, Jungblut B, Behl C, Terzic J, Dikic I. Ubiquitin-independent function of optineurin in autophagic clearance of protein aggregates. J Cell Sci. 2013; 126(Pt 2):580–92. [PubMed: 23178947]

Lin B, Peng EB. Retinal Ganglion Cells are Resistant to Photoreceptor Loss in Retinal Degeneration. PLoS ONE. 2013; 8(6):e68084. [PubMed: 23840814]

Lin B, Wang SW, Masland RH. Retinal ganglion cell type, size, and spacing can be specified independent of homotypic dendritic contacts. Neuron. 2004; 43(4):475–85. [PubMed: 15312647]

Liu YH, Tian T. Hypothesis of optineurin as a new common risk factor in normal-tension glaucoma and Alzheimer's disease. Medical Hypotheses. 2011; 77(4):591–2. [PubMed: 21764520]

Mabuchi F, Aihara M, Mackey MR, Lindsey JD, Weinreb RN. Regional optic nerve damage in experimental mouse glaucoma. Invest Ophthalmol Vis Sci. 2004; 45(12):4352–8. [PubMed: 15557443]

Maruyama H, Morino H, Ito H, Izumi Y, Kato H, Watanabe Y, Kinoshita Y, Kamada M, Nodera H, Suzuki H, Komure O, Matsuura S, Kobatake K, Morimoto N, Abe K, Suzuki N, Aoki M, Kawata A, Hirai T, Kato T, Ogasawara K, Hirano A, Takumi T, Kusaka H, Hagiwara K, Kaji R, Kawakami H. Mutations of optineurin in amyotrophic lateral sclerosis. Nature. 2010; 465(7295): 223–6. [PubMed: 20428114]

Meng Q, Xiao Z, Yuan H, Xue F, Zhu Y, Zhou X, Yang B, Sun J, Meng B, Sun X, Cheng F. Transgenic mice with overexpression of mutated human optineurin(E50K) in the retina. Molecular Biology Reports. 2011

Mori F, Tanji K, Toyoshima Y, Yoshida M, Kakita A, Takahashi H, Wakabayashi K. Optineurin immunoreactivity in neuronal nuclear inclusions of polyglutamine diseases (Huntington's, DRPLA, SCA2, SCA3) and intranuclear inclusion body disease. Acta Neuropathol. 2012

Morrison JC, Moore CG, Deppmeier LM, Gold BG, Meshul CK, Johnson EC. A rat model of chronic pressure-induced optic nerve damage. Exp Eye Res. 1997; 64(1):85–96. [PubMed: 9093024]

Morton S, Hesson L, Peggie M, Cohen P. Enhanced binding of TBK1 by an optineurin mutant that causes a familial form of primary open angle glaucoma. FEBS Lett. 2008; 582(6):997–1002. [PubMed: 18307994]

Nagabhushana A, Bansal M, Swarup G. Optineurin Is Required for CYLD-Dependent Inhibition of TNFalpha-Induced NF-kappaB Activation. PLoS ONE. 2011; 6(3):e17477. [PubMed: 21408173]

Ofverstedt LG, Hammarstrom K, Balgobin N, Hjerten S, Pettersson U, Chattopadhyaya J. Rapid and quantitative recovery of DNA fragments from gels by displacement electrophoresis (isotachophoresis). Biochim Biophys Acta. 1984; 782(2):120–6. [PubMed: 6722161]

Osawa T, Mizuno Y, Fujita Y, Takatama M, Nakazato Y, Okamoto K. Optineurin in neurodegenerative diseases. Neuropathology. 2011

Parisi V, Miglior S, Manni G, Centofanti M, Bucci MG. Clinical ability of pattern electroretinograms and visual evoked potentials in detecting visual dysfunction in ocular hypertension and glaucoma. Ophthalmology. 2006; 113(2):216–28. [PubMed: 16406535]

Paulus JD, Link BA. Loss of optineurin in vivo results in elevated cell death and alters axonal trafficking dynamics. PLoS ONE. 2014; 9(10):e109922. [PubMed: 25329564]

Porciatti V, Pizzorusso T, Maffei L. Electrophysiology of the postreceptoral visual pathway in mice. Doc Ophthalmol. 2002; 104(1):69–82. [PubMed: 11949810]

Prusky GT, West PW, Douglas RM. Behavioral assessment of visual acuity in mice and rats. Vision Res. 2000; 40(16):2201–9. [PubMed: 10878281]

Quigley HA. Neuronal death in glaucoma. Prog Retin Eye Res. 1999; 18(1):39–57. [PubMed: 9920498]

Quigley HA. New paradigms in the mechanisms and management of glaucoma. Eye (Lond). 2005; 19(12):1241–8. [PubMed: 15543179]

Quigley HA, Addicks EM. Chronic experimental glaucoma in primates. II. Effect of extended intraocular pressure elevation on optic nerve head and axonal transport. Invest Ophthalmol Vis Sci. 1980; 19(2):137–52. [PubMed: 6153173]

Quigley HA, Broman AT. The number of people with glaucoma worldwide in 2010 and 2020. Br J Ophthalmol. 2006; 90(3):262–7. [PubMed: 16488940]

Quigley HA, Green WR. The histology of human glaucoma cupping and optic nerve damage: clinicopathologic correlation in 21 eyes. Ophthalmology. 1979; 86(10):1803–30. [PubMed: 553256]

Rezaie T, Child A, Hitchings R, Brice G, Miller L, Coca-Prados M, Heon E, Krupin T, Ritch R, Kreutzer D, Crick RP, Sarfarazi M. Adult-onset primary open-angle glaucoma caused by mutations in optineurin. Science. 2002; 295(5557):1077–9. [PubMed: 11834836]

Sahlender DA, Roberts RC, Arden SD, Spudich G, Taylor MJ, Luzio JP, Kendrick-Jones J, Buss F. Optineurin links myosin VI to the Golgi complex and is involved in Golgi organization and exocytosis. J Cell Biol. 2005; 169(2):285–95. [PubMed: 15837803]

Sappington RM, Carlson BJ, Crish SD, Calkins DJ. The microbead occlusion model: a paradigm for induced ocular hypertension in rats and mice. Invest Ophthalmol Vis Sci. 2010; 51(1):207–16. [PubMed: 19850836]

Savinova OV, Sugiyama F, Martin JE, Tomarev SI, Paigen BJ, Smith RS, John SW. Intraocular pressure in genetically distinct mice: an update and strain survey. BMC Genet. 2001; 2:12. [PubMed: 11532192]

Shields MB. Normal-tension glaucoma: is it different from primary open-angle glaucoma? Current opinion in ophthalmology. 2008; 19(2):85–8. [PubMed: 18301279]

Sommer A. Ocular hypertension and normal-tension glaucoma: time for banishment and burial. Arch Ophthalmol. 2011; 129(6):785–7. [PubMed: 21670346]

Strain GM, Tedford BL. Flash and pattern reversal visual evoked potentials in C57BL/6J and B6CBAF1/J mice. Brain Res Bull. 1993; 32(1):57–63. [PubMed: 8319104]

Sudhakar C, Nagabhushana A, Jain N, Swarup G. NF-kappaB mediates tumor necrosis factor alpha-induced expression of optineurin, a negative regulator of NF-kappaB. PLoS One. 2009; 4(4):e5114. [PubMed: 19340308]

Sun W, Li N, He S. Large-scale morphological survey of mouse retinal ganglion cells. J Comp Neurol. 2002; 451(2):115–26. [PubMed: 12209831]

Tang Z, Zhang S, Lee C, Kumar A, Arjunan P, Li Y, Zhang F, Li X. An optic nerve crush injury murine model to study retinal ganglion cell survival. J Vis Exp. 2011; (50)

Tezel G, Li LY, Patil RV, Wax MB. TNF-alpha and TNF-alpha receptor-1 in the retina of normal and glaucomatous eyes. Invest Ophthalmol Vis Sci. 2001; 42(8):1787–94. [PubMed: 11431443]

Tyler CW. Specific deficits of flicker sensitivity in glaucoma and ocular hypertension. Invest Ophthalmol Vis Sci. 1981; 20(2):204–12. [PubMed: 7461923]

Wax MB, Tezel G, Edward PD. Clinical and ocular histopathological findings in a patient with normal-pressure glaucoma. Arch Ophthalmol. 1998; 116(8):993–1001. [PubMed: 9715678]

Wild P, Farhan H, McEwan DG, Wagner S, Rogov VV, Brady NR, Richter B, Korac J, Waidmann O, Choudhary C, Dotsch V, Bumann D, Dikic I. Phosphorylation of the Autophagy Receptor Optineurin Restricts Salmonella Growth. Science. 2011

Williams RW, Strom RC, Rice DS, Goldowitz D. Genetic and environmental control of variation in retinal ganglion cell number in mice. J Neurosci. 1996; 16(22):7193–205. [PubMed: 8929428]

WoldeMussie E, Ruiz G, Wijono M, Wheeler LA. Neuroprotection of retinal ganglion cells by brimonidine in rats with laser-induced chronic ocular hypertension. Invest Ophthalmol Vis Sci. 2001; 42(12):2849–55. [PubMed: 11687528]

Wong YC, Holzbaur EL. Optineurin is an autophagy receptor for damaged mitochondria in parkin-mediated mitophagy that is disrupted by an ALS-linked mutation. Proc Natl Acad Sci U S A. 2014; 111(42):E4439–48. [PubMed: 25294927]

Yu D, Ellis HM, Lee EC, Jenkins NA, Copeland NG, Court DL. An efficient recombination system for chromosome engineering in Escherichia coli. Proc Natl Acad Sci U S A. 2000; 97(11):5978–83. [PubMed: 10811905]

Zhu G, Wu CJ, Zhao Y, Ashwell JD. Optineurin negatively regulates TNFalpha- induced NF-kappaB activation by competing with NEMO for ubiquitinated RIP. Curr Biol. 2007; 17(16):1438–43. [PubMed: 17702576]

Highlights

- We generated a transgenic mouse model expressing disease-associated E50K mutation in optineurin
- This mouse model showed features of low pressure primary open angle glaucoma with aging
- E50K optineurin enhanced age-dependent loss of retinal ganglion cells and degenerating axons
- Compared to nontransgenic littermates, E50K optineurin mice showed functional visual impairment
- This mouse will be very useful to dissect disease mechanism in low pressure primary open angle glaucoma.

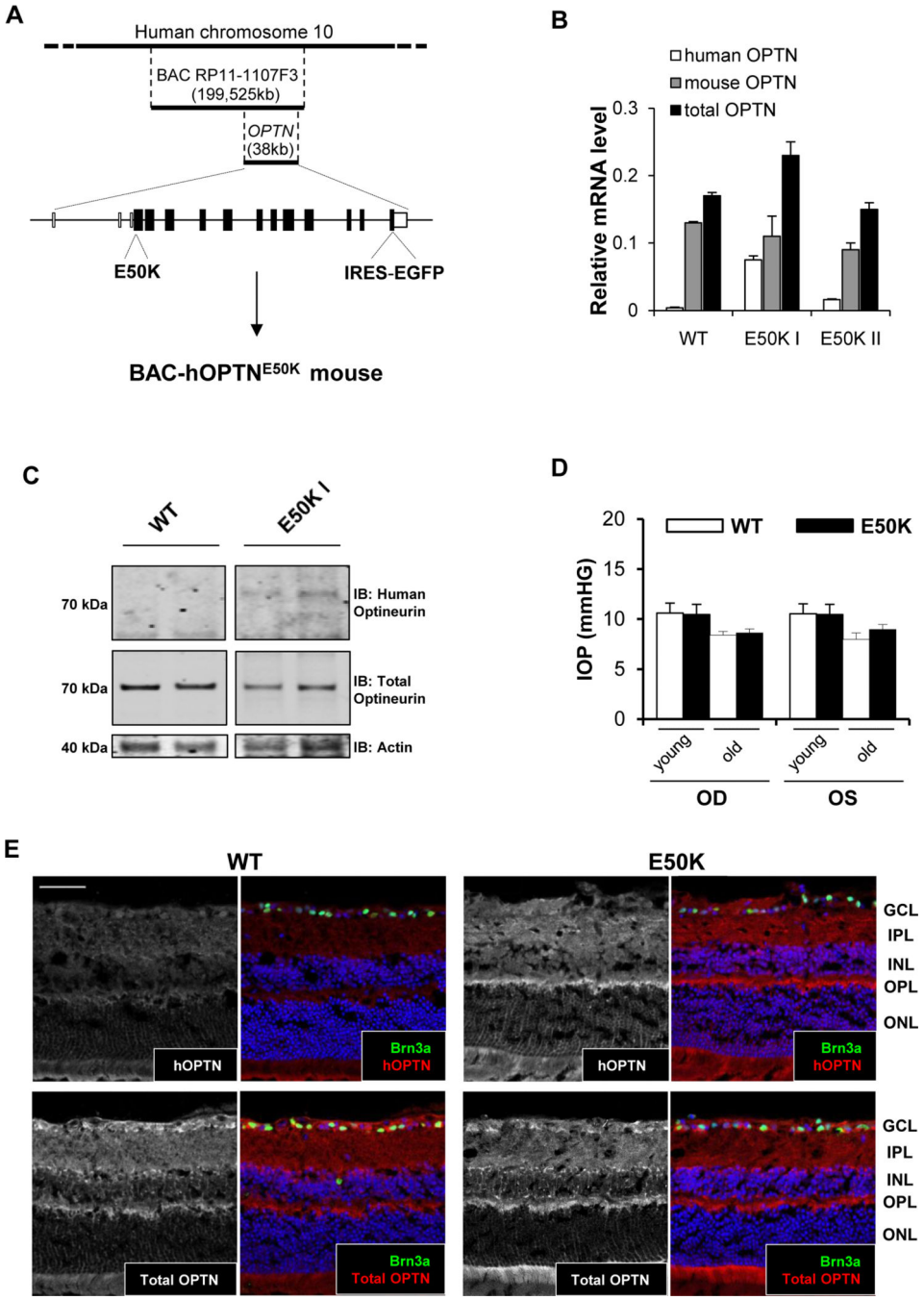

Figure 1. Generation and characterization of BAC hOPTN^{E50K} transgenic mice

(A) BAC transgenic mice expressing disease-associated mutant E50K human optineurin (BAC hOPTN^{E50K}) were generated by using genomic sequences coding for the optineurin promoter region and the human *OPTN* locus. (B) Quantification of human optineurin mRNA in 18-month old BAC hOPTN^{E50K} (E50K) and wildtype (WT) mice. E50K hOPTN overexpression was observed in line I, but not line II (E50K I, E50K II). Mouse OPTN (mOPTN) transcripts were similar in all three genotypes (n = 3 for each genotypes). Data presented as mean ± S.E.M. (C) Optineurin protein expression in isolated retinas from 18

month old mice were analyzed by immunoblot analysis. Shown are two different animals for each genotype. Using an antibody that recognizes human optineurin but not mouse optineurin, the expression of the BAC transgene was observed in retinas from line I of BAC hOPTN^{E50K} mice.

(D) In young, 2-3 month old E50K and WT mice (n = 5 per genotype), the IOP was similar between the two gentoypes (p = 0.77) and between the right (OD) and left (OS) eyes within each genotype (p = 0.39 for E50K; p = 0.88 for WT). Similarly, in aged 18-month old E50K (n = 11) and WT (n = 10) mice, the IOP was not different between different genotypes (p = 0.05) or between the right and left eyes within each genotype (p = 0.39 for E50K; p = 0.20 for WT). (E) hOPTN expression pattern is similar to endogenous mouse OPTN. Immunofluorescent labeling in retina cryosections from 18-month old wildtype (WT) or BAC-hOPTN^{E50K} (E50K) mice. Brn3a was used as a marker for retinal ganglion cells. Using an antibody specific for human optineurin (hOPTN), immunoreactivity was observed only in BAC-hOPTN^{E50K} but not wildtype retinas (top panels). Mouse OPTN expression was observed with a different antibody that recognizes both human and mouse optineurin (bottom panels). n=3 animals per genotype. Scale bars 50 m.

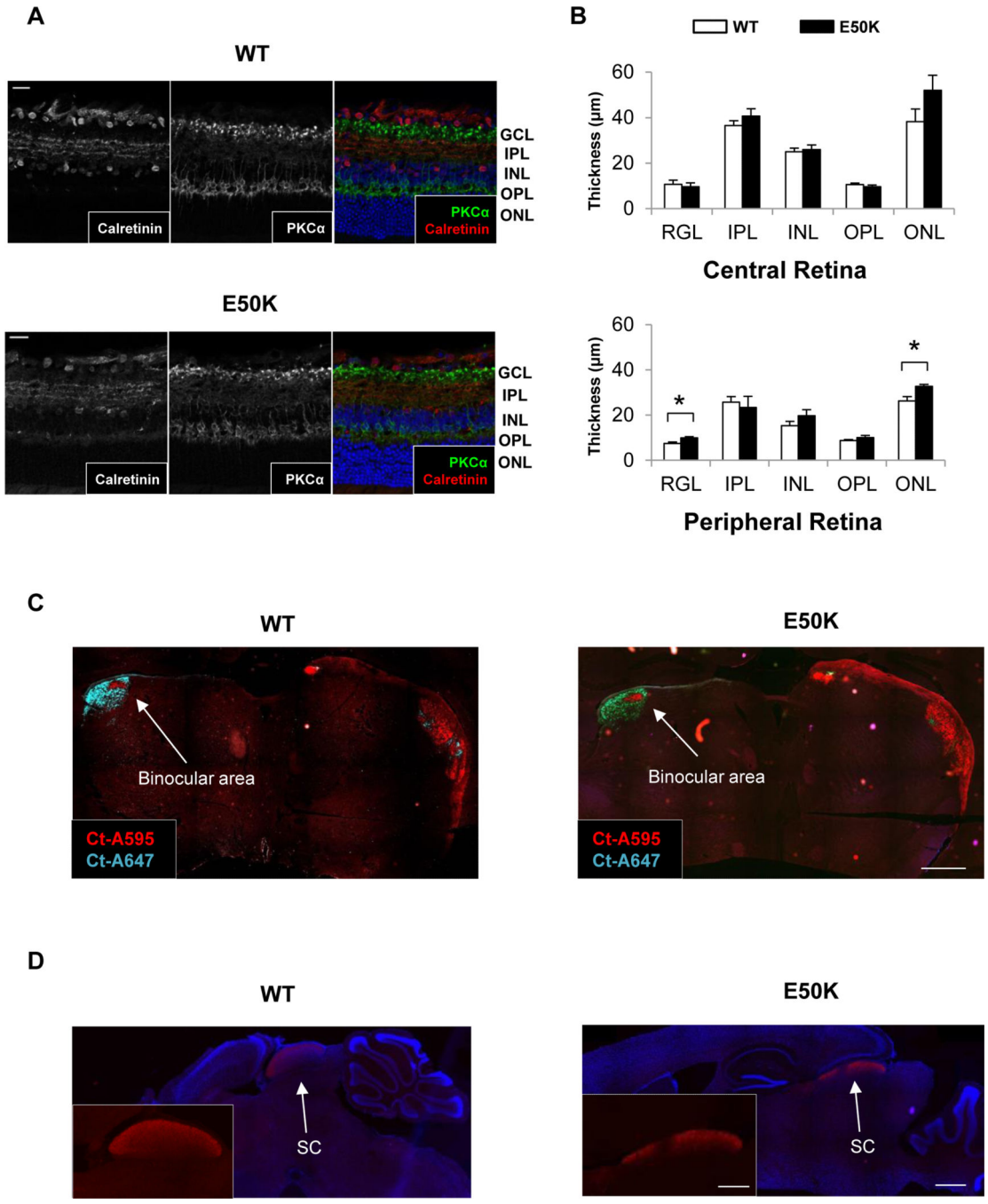

Figure 2. BAC hOPTN^{E50K} retinas exhibit normal retina layers and RGC axon projections

(A) Normal gross histological layers in retinas from 18-month old BAC hOPTN^{E50K} (E50K) and wildtype (WT) mice. PKCα staining (green) labeled bipolar cells while calretinin (red) identifies amacrine cells, RGC, and the three dendritic strata between sublaminae of the IPL. No significant decreases in photoreceptors nuclei were observed in the ONL. Scale bar, 50 m. (B) Quantitation of retinal layers show they were grossly similar for both genotypes, except GCL and ONL layers in peripheral BAC hOPTN^{E50K} retinas, which were slightly increased. Data presented as mean ± S.E.M. (C) Fluorescently-labeled cholera toxin (ct) was

used as an anterograde tracer. Ct-A595 (red) was injected into the right eye while ct-A647 (cyan) was injected into the left eye to visualize ipsilateral and contralateral RGC axonal projections in the brains of old (>18 months) BAC hOPTN^{E50K} and wildtype mice (n = 3 animals per genotype). Coronal brain sections showed normal RGC terminals from both eyes are found in the binocular area labeled by both red and cyan fluorescence. (D) Sagital brain sections showing Ct-A595 in the superior colliculus (SC) with blue DAPI nuclear stain. Occasional segmental loss of fluorescence is observed in BAC hOPTN^{E50K} mice. Scale bar, 1 mm, 500 μm (high magnification).

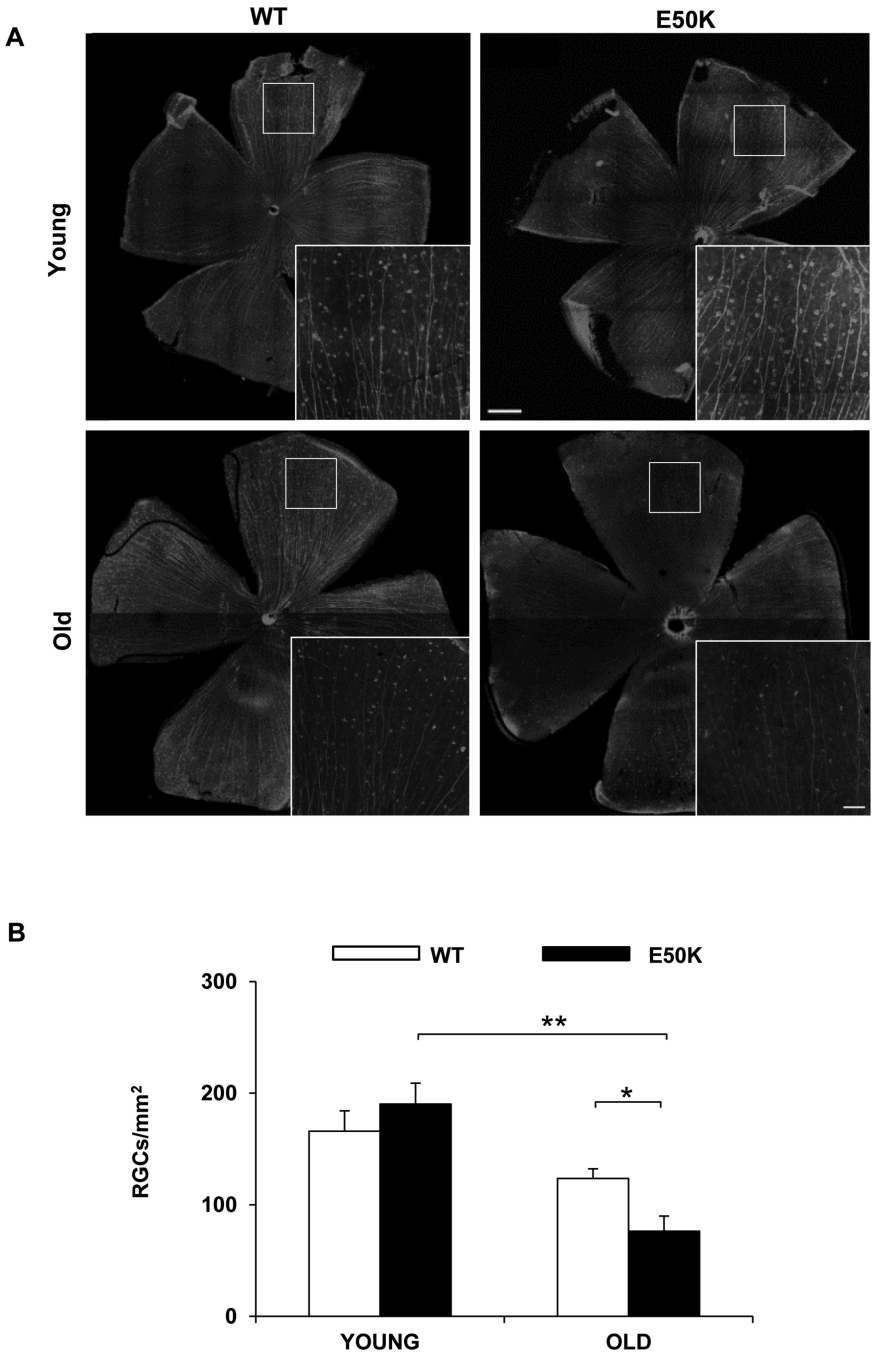

Figure 3. ression of E50K optineurin induced an age-related loss of retinal ganglion cells

(A) Representative retinal flatmounts from young and aged wildtype (WT) and BAC hOPTN^{E50K} (E50K) mice are shown. RGCs are labeled with the SMI-32 antibody. Magnified regions of retinas are indicated by the white box. RGC axons course toward the center of the retina to exit the eye through the optic nerve. Aged BAC hOPTN^{E50K} retinas exhibited fewer RGCs with smaller somas and thinner axons than WT controls. Scale bar, 500 m, 100 m (high magnification). (B) Quantitative analysis of RGC density showing a

decrease in aged BAC hOPTN^{E50K} mice. Data represent means ± SEM, 5 animals per genotype per age group, * $p<0.02$, ** $p < 0.001$.

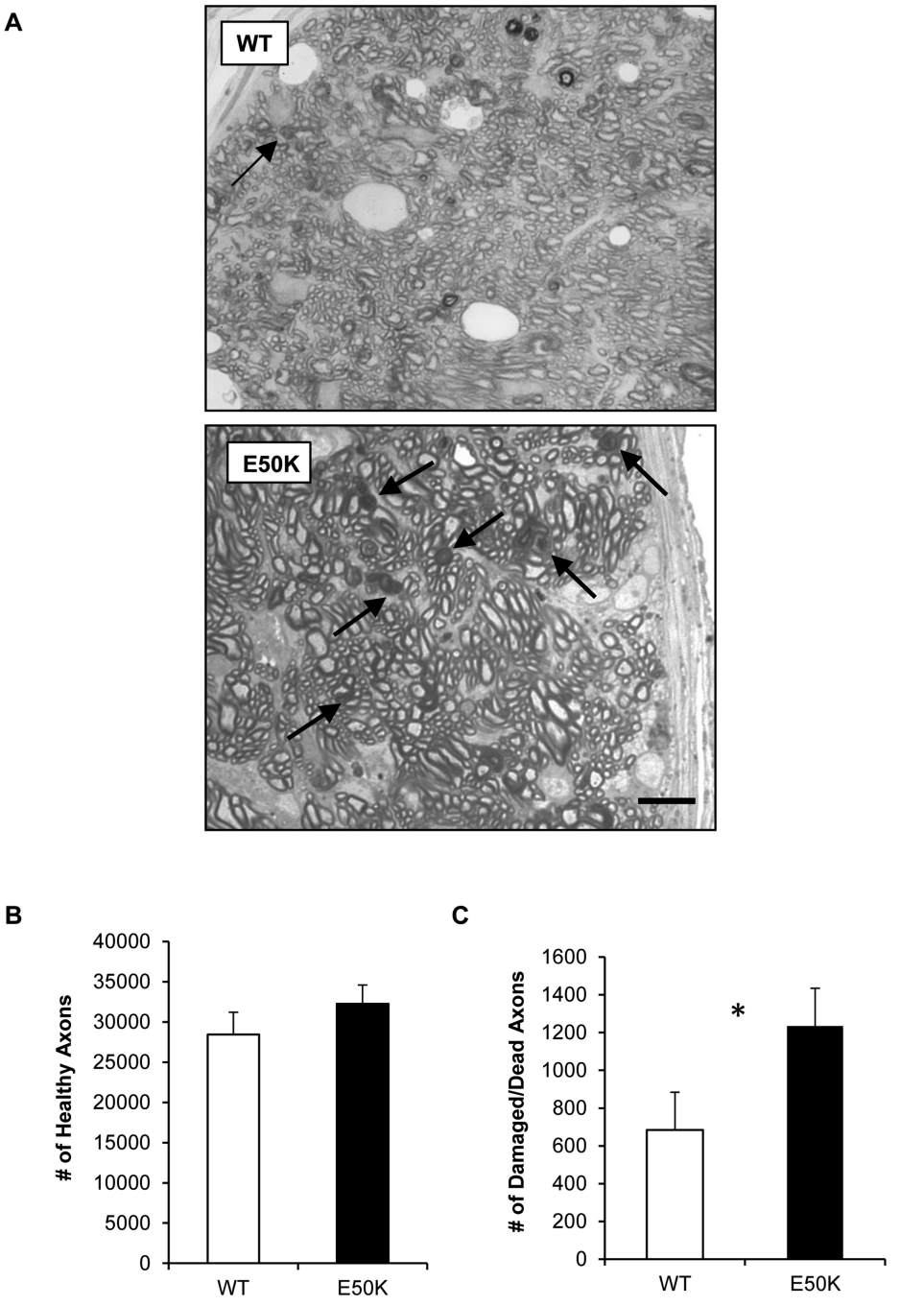

Figure 4. E50K optineurin is associated with a higher number of damaged axons

(A) Paraphenylenediamine (PPD) staining in representative optic nerve cross sections from wildtype (WT) and BAC hOPTN^{E50K} (E50K) mice. PPD stains the axoplasm of damaged or dead axons (arrows). Scale bar, 10 μm. (B) Axon counts of healthy axons showed no significant difference between the two genotypes ($p = 0.33$). However, there was a higher number of damaged or degenerated axons by PPD staining (* $p = 0.03$) in BAC hOPTN^{E50K} mice (n = 4 animals, 8 optic nerves) than wildtype littermates (n = 6 animals, 11 optic nerves). Data represent means ± SEM.

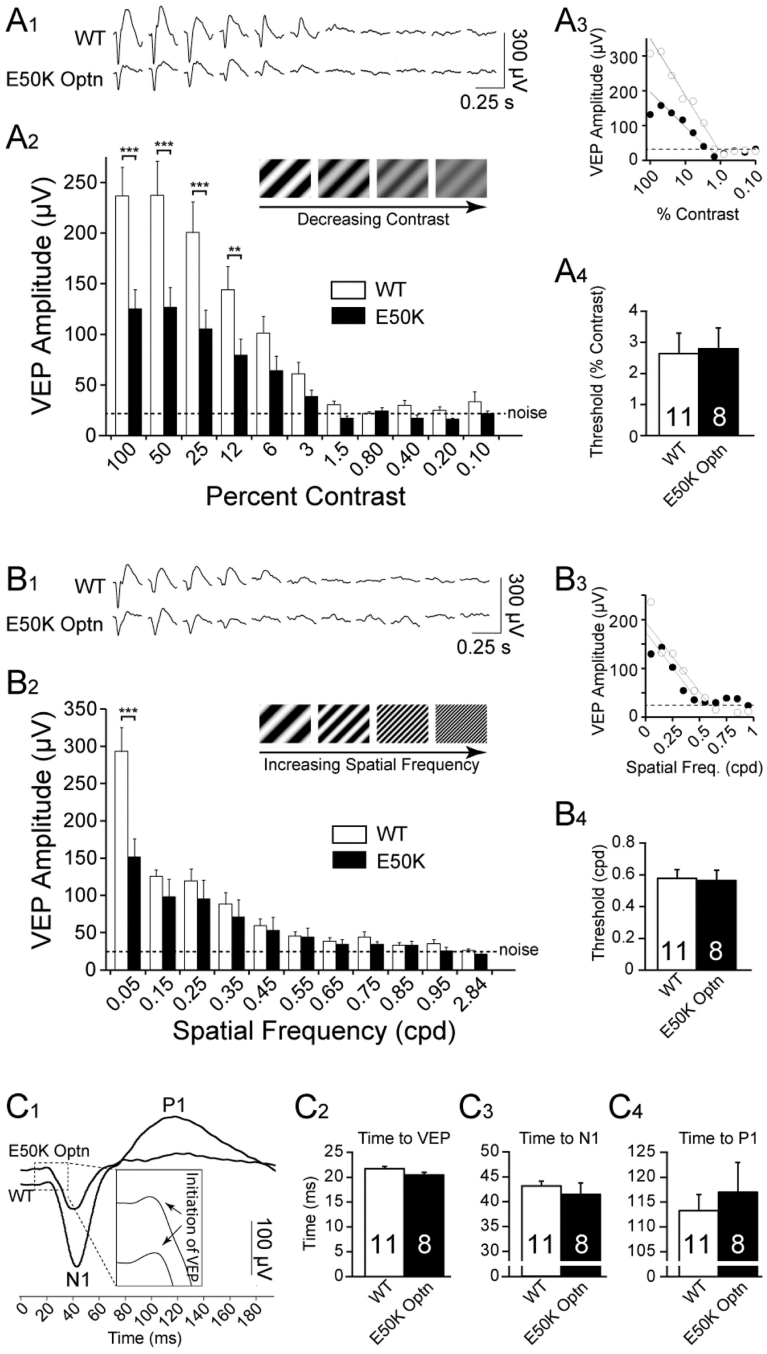

Figure 5. Mice expressing E50K human mutant optineurin demonstrate functional visual impairment

(A) Contrast sensitivity testing by VEP. (A1) Representative VEP waveforms recorded. (A2 & A3) Visual responsiveness to patterned stimuli of decreasing contrast was significantly diminished in BAC hOPTN^{E50K} mice compared to wildtype littermates between the range of 100 to 12 percent contrast ($p = 0.008$). Note that the x-axis is plotted logarithmically. (A4) Logarithmic regression shows normal contrast sensitivity threshold. (B) Visual acuity testing by VEP as spatial frequency in cycles per degree (cpd). (B1) Representative VEP waveforms. (B2 & B3) VEP responses were reduced at 0.05 cpd in BAC hOPTN^{E50K} mice

($p < 0.001$), but were comparable at other spatial frequencies to wildtype littermates. (B4) Linear regression showed similar visual acuity threshold for both genotypes. (C) VEP waveform latency revealed no delay in nerve conduction in 18-month old BAC hOPTN^{E50K} mice. (C1) The averaged VEP waveform shows the initiation of the VEP which is when the visual signal was first detected in the primary visual cortex following visual stimulation. (C2-C4) There was no temporal delay in the initiation of the visual cortical response (Time to VEP), the negative peak (Time to N1) or positive peak (Time to P1) following visual stimulation. n = 11 WT, n = 8 for E50K, data represent means ± SEM. **$p < 0.01$, ***$p < 0.001$.